Discrimination of Real and Virtual Surfaces with Sinusoidal and Triangular Gratings Using the Fingertip and Stylus

Matthew B. Kocsis, *Member*, *IEEE*, Steven A. Cholewiak, Ryan M. Traylor, Bernard D. Adelstein, *Senior Member*, *IEEE*, E. Daniel Hirleman, and Hong Z. Tan, *Senior Member*, *IEEE*

Abstract—Two-interval two-alternative forced-choice discrimination experiments were conducted separately for sinusoidal and triangular textured surface gratings from which amplitude (i.e., height) discrimination thresholds were estimated. Participants (group sizes: $n = 4$ to 7) explored one of these texture types either by fingertip on real gratings (Finger real), by stylus on real gratings (Stylus real), or by stylus on virtual gratings (Stylus virtual). The real gratings were fabricated from stainless steel by an electrical discharge machining process while the virtual gratings were rendered via a programmable force-feedback device. All gratings had a 2.5-mm spatial period. On each trial, participants compared test gratings with 55, 60, 65, or $70\ \mu\mathrm{m}$ amplitudes against a 50-$\mu\mathrm{m}$ reference. The results indicate that discrimination thresholds did not differ significantly between sinusoidal and triangular gratings. With sinusoidal and triangular data combined, the average (mean $\pm$ standard error) for the Stylus-real threshold $(2.5 \pm 0.2\ \mu\mathrm{m})$ was significantly smaller $(p < 0.01)$ than that for the Stylus-virtual condition $(4.9 \pm 0.2\ \mu\mathrm{m})$. Differences between the Finger-real threshold $(3.8 \pm 0.2\ \mu\mathrm{m})$ and those from the other two conditions were not statistically significant. Further studies are needed to better understand the differences in perceptual cues resulting from interactions with real and virtual gratings.

Index Terms—Haptic texture perception, real texture, virtual texture, amplitude discrimination

1 Introduction

Haptic texture perception has attracted much research attention since at least 1925 [1]. To facilitate such research, a key question one may ask is: What would it take for us to easily manipulate the feel of surface textures? An understanding of the physical determinants, the perceptual dimensionality, and the neural mechanisms of texture perception is fundamental to addressing this question (e.g., [2], [3], [4], [5]).

To study the physical determinants and the neural mechanisms of texture perception, texture samples with well-controlled surface features are needed. For example, a multidimensional scaling study using 17 texture patches (sandpaper, velvet, etc.) found that a three-dimensional (3D) perceptual space provided a satisfactory representation of perceived similarity judgment data [5]. The dimensions were roughness smoothness, hardness-softness, and possibly "springiness" of the texture surfaces. Of the three dimensions proposed by Hollins et al. [5], much is known about the roughness-smoothness dimension (see [6], for a recent review). Typical stimuli used for roughness studies include sandpapers with varying grit numbers (e.g., [7]), metal plates with linear grooves (e.g., [8], [9]), raised dots with controlled height and density (e.g., [10], [11], [12]), and dithered cylindrical raised elements [6].

An alternative to the aforementioned stimuli is to use 1D sinusoidal gratings with controlled amplitude and spatial wavelength, since, according to Fourier analysis, sinusoidal signals can be viewed as the building blocks of any surface profile. It is, however, extremely expensive and time consuming to fabricate high definition (i.e., high precision, fine resolution) sinusoidal surfaces. We are aware of only two research groups who used such stimuli previously [9], [13], [14]. On the other hand, it is straightforward to render microgeometric features such as virtual sinusoidal gratings using software-programmable force-feedback devices (e.g., [15], [16], [17]). Haptic interfaces are similarly well suited for modulating other perceptual features such as hardness/softness and springiness (e.g., [18], [19]).

Given the time and cost associated with the fabrication of high-definition real surface gratings, it should be more desirable to use virtual textures. Furthermore, it is relatively easy to alter the parameters of virtual textured surfaces so

- *M.B. Kocsis is with Aircell, 303 S Technology Ct, Bldg A, Broomfield, CO 80021. E-mail: mattkocsis@alumni.purdue.edu.*
- *S.A. Cholewiak is with the Department of Psychology, Rutgers University, 152 Frelinghuysen Road, Piscataway, NJ 08854. E-mail: scholewi@rutgers.edu.*
- *R.M. Traylor is with the Battelle Memorial Institute, Battelle Huntsville Operations, 7047 Old Madison Pike, NW Ste 340, Huntsville, AL 35806. E-mail: ryantraylor@alumni.purdue.edu.*
- *B.D. Adelstein is with the Human Systems Integration Division, NASA Ames Research Center, Bernard D. Adelstein/Mail Stop 262-2, PO Box 1, Moffett Field, CA 94035-0001. E-mail: Bernard.D.Adelstein@nasa.gov.*
- *E.D. Hirleman is with the School of Engineering, University of California, 5200 N. Lake Road, Merced, CA 95343. E-mail: dhirleman@ucmerced.edu.*
- *H.Z. Tan is with the Haptic Interface Research Laboratory, School of Electrical and Computer Engineering, Purdue University, Electrical Engineering Building, 465 Northwestern Ave., West Lafayette, IN 47907-2035. E-mail: hongtan@purdue.edu.*

Manuscript received 24 Sept. 2010; revised 30 Apr. 2012; accepted 14 May 2012; published online 5 June 2012.
Recommended for acceptance by V. Hayward.
For information on obtaining reprints of this article, please send e-mail to: toh@computer.org, and reference IEEECS Log Number TH-2010-09-0061.
Digital Object Identifier no. 10.1109/ToH.2012.31.

that more efficient experimental methods such as adaptive psychophysical procedures can be used. To do so requires that the following two issues be resolved: 1) What does it mean for real or virtual textures to have "high definition" sufficient enough for studying human perception of texture? 2) How valid is it to use virtual textures instead of real ones for studying human texture perception?

If the goal is to measure the amplitude detection or discrimination threshold for surface gratings, then the answer to the first question is that the resolution of the textured surfaces needs to be on the order of single microns [13], [14]. Louw et al. found the detection thresholds of real Gaussian profiles to vary from $1\ \mu\mathrm{m}$ to 8 mm from the narrowest $(\sigma : 150\ \mu\mathrm{m})$ to the broadest $(\sigma : 240\ \mathrm{mm})$ Gaussian-shaped profiles, regardless of whether the shapes were convex or concave [13]. The thresholds were then converted to equivalent amplitude detection thresholds for sinusoidal gratings by matching Gaussian and sinusoidal profiles with the same maximum slope (cf. [14]), resulting in sinusoidal gratings threshold estimates of 0.64 to $4.99\ \mu\mathrm{m}$ for spatial periods of 2.5 to 10.0 mm. For amplitude discrimination, Nefs et al. reported a threshold as small as $2\ \mu\mathrm{m}$ (reference amplitude: $12.8\ \mu\mathrm{m}$, spatial period: 2.5 mm) for sinusoidal gratings using active dynamic touch [14]. Nefs et al. also found that amplitude discrimination improved with increasing spatial period (from 2.5 to 10.0 mm). (Note that the thresholds summarized above are for direct finger-on-texture contact.)

Lederman [9] demonstrated the inadequacy of traditional fabrication techniques for producing surface features of sufficient precision and resolution in haptics research. In that study, aluminum surfaces with square-shaped gratings were fabricated using either a cutting bit or an electrical discharge machining (EDM) technique. The surfaces looked quite different under a scanning electron microscope (see [9, Figs. 5 and 6]) and produced different perceived roughness curves as a function of nominal groove width. It was reported that lands and grooves were cut to within 50 and $25\ \mu\mathrm{m}$ of their nominal values with the cutting bit and EDM, respectively. This accuracy was clearly inadequate in light of the single micron detection and discrimination thresholds measured by Louw et al. [13], and Nefs et al. [14], and the different surfaces were indeed judged differently in a magnitude estimation task [7].

In the present study, stainless steel textured surface samples, with better accuracy and resolution, were fabricated by an improved EDM technique. An additional polishing step was applied to ensure the smoothness of the resulting gratings, to reduce the influence of friction on amplitude discrimination. The final quality of these real textured surfaces was verified by surface profilometry.

For virtual surface rendering, it should be noted that most commercially available force feedback devices have a position resolution on the order of $10\ \mu\mathrm{m}$ or larger. For example, the Omega.3 (ForceDimension) and the PHANToM Desktop (SensAble Technologies), respectively, have nominal position resolutions of < 10 and $23\ \mu\mathrm{m}$ (device specifications accessed online on 28 April 2012). These values are likely due to encoder resolution limitations but do not take linkage or transmission compliance into account. In the present study, we used a custom-built force-feedback device with sensor resolution verified for $1.5\ \mu\mathrm{m}$ of end-point displacement ([20, p. 5]; Fig. 4). The accuracy of virtual surface gratings rendered with this device was evaluated by recording the stylus position during lateral stroking and performing a Fourier analysis to examine the spectral components of the surface height profile.

To address the second issue of whether virtual instead of real textures can be used for the study of texture perception, we compared discrimination thresholds obtained with real and virtual textures. Ideally, one would prefer to render virtual textures that cannot be distinguished from real textures. It is however almost impossible to demonstrate the equivalence experimentally, short of making interfaces to real and virtual objects that feel, look, and sound identical to participants. Even so, several studies have compared user performance using similar tasks implemented in real and virtual environments, and the results are mixed. For example, Buttolo et al. [21] reported almost identical task completion time in direct and virtual manipulations. In a study by Unger et al. [22], an interface for a real peg-in-hole task was built to be like the interface to a magnetic levitation haptic device, and it was found that participants performed faster inserting a real peg in a real hole than when using a maglev device with a virtual peg and hole. A further study by Unger et al. [23] found that during a roughness estimation task with virtual textures rendered on a magnetic levitation device, participants showed the same psychophysical functions as with a real stylus on real textured surfaces (reported in [6]).

Metrics other than task completion time and psychophysical functions have also been employed to compare performance between real and virtual environments. West and Cutkosky [24] asked observers to count the number of 1D sinusoidal cycles on real and virtual surfaces. The best accuracy was found using fingertips on real textured surfaces, followed by a stylus on real textures, with the lowest accuracy for a stylus on virtual textures. Greenish et al. [25] demonstrated that tissue identification accuracy for a real tissue-cutting task was similar to a simulated cutting task in which force data recorded during real cutting were played back through a custom-designed haptic device. More recently, O'Malley and Goldfarb [26] concluded that size-identification tasks performed with a haptic interface capable of sufficient force output can approach the percent-correct level in a real environment, but the accuracy of size-discrimination tasks performed in a virtual environment was consistently lower than that in a real environment.

Even though results comparing performance in real and virtual environments remain somewhat inconsistent, there is a growing trend of studying haptic texture perception using simulated objects and properties, presumably because it is much easier to create virtual objects than real ones. For example, Ikei and Shiratori showed that a pin-array attached to a force-feedback interface enhanced tactile texture perception [27]. Kyung et al. investigated the roles of kinesthetic force feedback, tactile pressure distribution, vibration, and skin stretch in displaying surface properties using an integrated mouse-type haptic display [28]. Campion et al. showed, using a five-bar

Fig. 1. A stainless steel block with a sinusoidal surface grating ($\lambda = 2.5$ mm, $A_3 = 65$ μm).

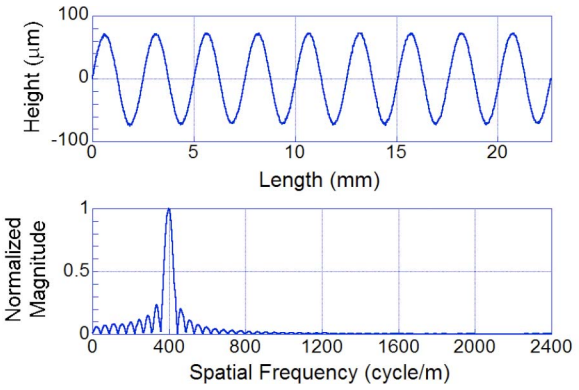

Fig. 2. (Top) Profilometry surface height $h(x)$ of the reference sinusoidal grating sample ($\lambda = 2.5$ mm, $A_3 = 65$ μm). (Bottom) Normalized spectral magnitude of the measured height profile in the top panel.

pantograph-type of haptic display, that both the amplitude and friction coefficient of sinusoidal friction gratings contribute to perceived roughness of the gratings [29]. Samra et al. found two diverging patterns of roughness perception for a rotating spiral brush attached to a force-feedback device [30], [31]. Our own previous studies on haptic texture perception have used virtual textures extensively (e.g., [32], [17], [33], [20]).

In the present study, we examined whether similar amplitude discrimination thresholds can be obtained with high-definition real and virtual surface gratings using (nearly) identical experimental methods. We chose amplitude discrimination threshold as a performance metric because it is a standard measure in psychophysics and therefore our results can be readily compared to those available in the literature. We contrasted amplitude discrimination thresholds from three experimental conditions: stroking a real textured surface with a fingertip (Finger real), stroking a real grating with a stylus (Stylus real), and stroking a virtual surface grating with a stylus (Stylus virtual). To the extent that similar thresholds exist for real and virtual textured surfaces, we may conclude that functionally, it is valid to study human texture perception using synthesized virtual textured surfaces rendered with a force-feedback device.

We used both sinusoidal and triangular gratings that varied in one dimension in our study. We chose sinusoidal gratings because any surface profile can be decomposed into a sum of sinusoidal gratings via Fourier analysis. The choice of triangular gratings was based on our interest in studying surface gratings with greater spectral complexity and consequently higher spatial frequency contents than the sinusoidal gratings. We wanted to assess whether amplitude discrimination thresholds were similar (or different) for real sinusoidal and triangular gratings, and whether they were likewise similar (or different) for virtual gratings.

There were three main objectives of the present study. First, we wanted to compare amplitude discrimination thresholds obtained with real and virtual surface gratings defined by the same height profiles. This comparison is part of our ongoing validation of our "ministick" haptic interface device. Second, we wanted to investigate the effect of exploration method (fingertip versus stylus) on the thresholds. Finally, we were interested in comparing the thresholds for sinusoidal and triangular gratings obtained under the same experimental conditions to see whether the complexity of spectral contents affected discrimination thresholds. In the following sections, we present the methods and results and conclude with a discussion.

2 Methods

In this section, we describe the real and virtual texture gratings, their validation, experimental procedures, data analyses, and participants.

2.1 Real Texture Gratings

The real grating samples were machined out of stainless steel blocks using a wire EDM process. The dimension of each block was 100 mm (Length) $\times$ 30 mm (Width) $\times$ 15 mm (Height). It is a time-consuming process to fabricate the samples and we limited our experiments to one value of spatial period ($\lambda = 2.5$ mm).[1] There was one reference amplitude ($A_0 = 50$ μm) and four comparison amplitudes ($A_1 = 55$ μm, $A_2 = 60$ μm, $A_3 = 65$ μm, $A_4 = 70$ μm) for both the sinusoidal and triangular gratings.

The profile of a high-precision sinusoidal grating is

$$h_{\sin}(x) = A_{\sin} \sin(2\pi x/\lambda), \tag{1}$$

where $h_{\sin}$ denotes the vertical (z) height of the sinusoidal grating surface, x the horizontal position, $A_{\sin}$ the grating's sinusoidal amplitude, and λ the spatial period. Fig. 1 shows a sinusoidal grating block with $A_3 = 65$ μm. The profile of a high-precision triangular grating is

$$h_{tri}(x) = \begin{cases} \dfrac{4A_{tri}}{\lambda} x_{\mathrm{mod}} - A_{tri} & \text{if } x_{\mathrm{mod}} < \dfrac{\lambda}{2} \\ -\dfrac{4A_{tri}}{\lambda}\left(x_{\mathrm{mod}} - \dfrac{\lambda}{2}\right) + A_{tri} & \text{if } x_{\mathrm{mod}} \geq \dfrac{\lambda}{2}, \end{cases} \tag{2}$$

where h_{tri} denotes the height of the triangular grating surface, A_{tri} the grating's triangular amplitude, and $\mathrm{x_{mod}} = \mathrm{x}$ modulo λ.

After the sample surfaces were sandblasted clean, a surface profilometer (model Surtronic 3plus, Taylor Hobson, United Kingdom) was used to verify the surface geometry of each grating samples at a spatial sampling period of 1 μm. The tip of the profilometer was moved along the length of the block (x-axis) while maintaining contact with the surface.

1. This spatial period corresponded to the interelement spacing that produced the greatest perceived roughness, according to the roughness judgments reported in [6] and [34].

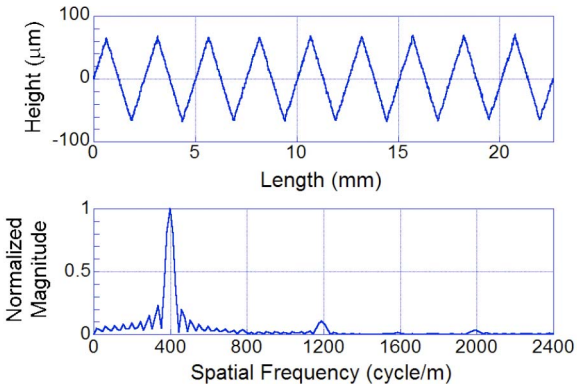

Fig. 3. (Top) Profilometry surface height $h(x)$ of a triangular grating sample ($\lambda = 2.5$ mm, $A_3 = 65$ μm). (Bottom) Normalized spectral magnitude of the measured height profile shown in the top panel. (Modified from [35], Fig. 1, © 2007 IEEE).

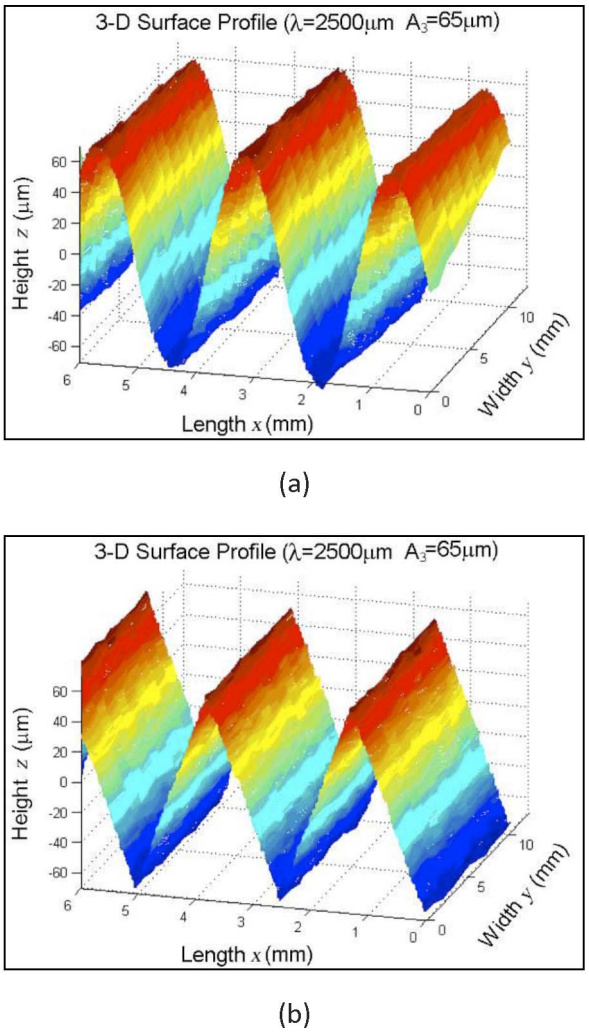

Fig. 4. 3D raster-scan plots of real texture gratings with a spatial period of $\lambda = 2.5$ mm and an amplitude of $A_3 = 65$ μm for (a) a sinusoidal grating (Modified from [36], Fig. 5, © 2006 IEEE) and (b) a triangular grating (Modified from [35], Fig. 2, © 2007 IEEE). Both plots show multiple lengthwise profilometer scans taken at several displacements along the width of the grating.

The height trace $h(x)$ along a fixed y position could then be plotted and analyzed. Fig. 2 shows the $h(x)$ plot for a sinusoidal grating with $A_3 = 65$ μm and its Fourier transform. It can be seen that the EDM produced a very "clean" sinusoidal profile. There were no discernable harmonics at multiples of 400 cycles/m $(1/\lambda)$. The side lobes were associated with the sinc function due to the finite sample length of $h(x)$.

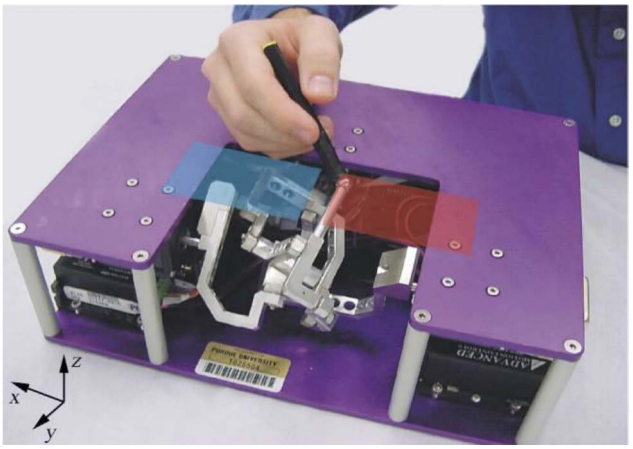

Fig. 5. The ministick force-feedback haptic device. The magenta and cyan patches are an illustration that indicates (roughly) the locations of the virtual textured gratings being discriminated.

Fig. 3 shows the height map for a triangular grating with $A_3 = 65$ μm and its Fourier transform. Mathematically, the Fourier series of a triangular waveform is

$$A_{tri}\left(\frac{8}{\pi^2}\right)\left\{\sin\frac{2\pi x}{\lambda} + \left(\frac{1}{3}\right)^2 \sin 3\frac{2\pi x}{\lambda} + \left(\frac{1}{5}\right)^2 \sin 5\frac{2\pi x}{\lambda} + \cdots\right\}. \tag{3}$$

Therefore, the spectral components of a triangular profile include its fundamental, a third harmonic with a magnitude that is 1/9 of that of the fundamental, a fifth harmonic at 1/25 of the amplitude of the fundamental, etc., as evident in the bottom plot of Fig. 3. Other than the side lobes visible primarily around the fundamental component due to the finite signal length, there was no discernable noise in the Fourier spectrum.

The profilometer was also used to measure parallel profiles in the x direction along several y values to check the grating consistency along the width of the block (y-axis). The traces were then combined to form a 3D raster-scan plot of the grating sample. Fig. 4a shows such a plot for the sinusoidal grating shown in Figs. 1 and 2, while Fig. 4b shows a 3D raster-scan plot of the triangular grating shown in Fig. 3. Further Fourier analysis confirmed that each sinusoidal and triangular grating sample was consistent along its width.

2.2 Virtual Texture Gratings

The virtual gratings were rendered by a 3-degree of freedom (DOF) force-feedback device called the "ministick" [37]. The device is based on the mechanical linkage described by Adelstein [38] and implemented by Steger et al. [39], but with a revised ethernet-enabled embedded controller for stand-alone operation designed and built by Traylor et al. [37]. The ministick has a calibrated position resolution of 1.5 μm [20]. Its force commands are updated at 2 kHz. Fig. 5 shows a user interacting with virtual haptic objects using a stylus.

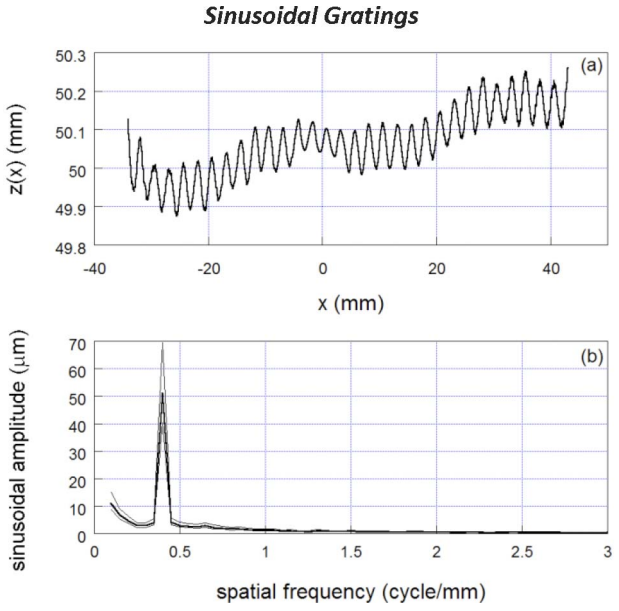

Fig. 6. Analysis of virtual sinusoidal gratings. (a) Recorded temporal position of the stylus $z(t)$ resampled with respect to x for a sinusoidal grating with $A_0 = 50\ \mu\text{m}$ and $\lambda = 2.5$ mm. (b) Averaged spatial spectrum magnitude in grating height (darker center line) with 95 percent confidence upper and lower bounds (upper and lower lighter lines, respectively).

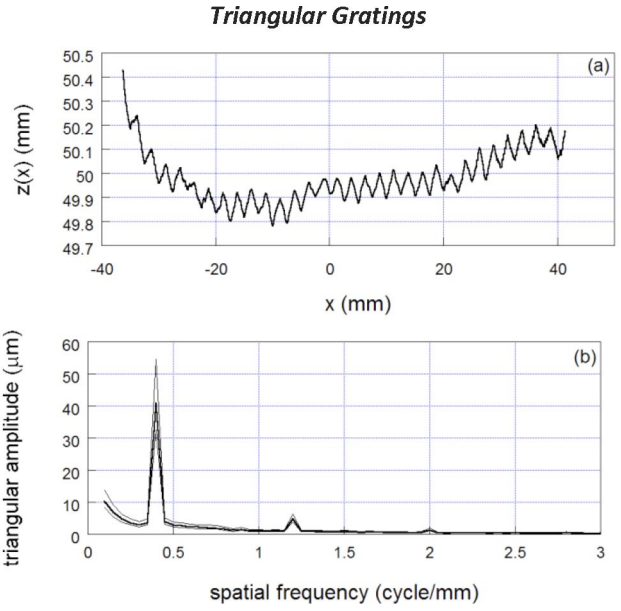

Fig. 7. Analysis of virtual triangular gratings. (a) Recorded temporal position of the stylus $z(t)$ resampled with respect to x for a triangular grating with $A_0 = 50\ \mu\text{m}$ and $\lambda = 2.5$ mm. (b) Averaged spatial spectrum magnitude in grating height (darker center line) with 95 percent confidence upper and lower bounds (upper and lower lighter lines, respectively).

The height map of the virtual sinusoidal and triangular gratings was the same as (1) and (2) where $\lambda = 2.5$ mm and A_{sin} or A_{tri} was selected on the fly from the five amplitude values of 50, 55, 60, 65, or 70 μm. The feedback force was calculated as

$$F_z = \begin{cases} K \times \left[h(x) - p_z\right] & when\ p_z < h(x) \\ 0 & otherwise, \end{cases} \tag{4}$$

where the force F_z always pointed up (i.e., no tangential component F_{x} or F_{y}), $h(x)$ was the surface height for the sinusoidal or triangular gratings, p_z was the z position of the ministick stylus tip, and the stiffness coefficient K was kept constant at 2.0 kN/m.

The characteristics of the virtual gratings were evaluated by analyzing recorded position signals in the spatial frequency domain. Specifically, $x(t)$ and $z(t)$ were recorded at a sampling rate of 2 kHz while the virtual grating was stroked at a uniformly paced speed of 15 mm/s. In order to compute the power spectral density of $z(x)$ to examine the *spatial* frequency content of the recorded surface height signal, cubic spline interpolation was used to resample $z(t)$ at a uniformly spaced x-axis sampling period of $\Delta x = 5\ \mu$m.

Fig. 6a provides an example of $z(x)$, recorded for a single stroke of the virtual sinusoidal grating, showing the peak-to-peak changes in individual bump height as well as the lower frequency variation in penetration depth along the z-axis that are typical of user interaction with virtual surfaces. To assess this variability, power spectrum along with statistical confidence estimates were made for the resampled $z(x)$ data as follows: After removing the first and last 500 interpolated (i.e., 2.5 mm along x-axis) points from each stroke to reduce the transients associated with initial and final grating contact, periodograms were calculated from consecutive 2,000-point intervals. With three periodograms obtained per stroke, the nine strokes of the sinusoidal grating yielded a total of 27 independent periodograms that were then averaged within each spatial frequency bin. Multiplying the resulting mean spectral density in each bin by the 0.05 cycle/mm bin width results in the mean-square amplitude. Taking the square root of the mean squares and multiplying by $\sqrt{2}$ provides an estimate of the equivalent amplitude of the sinusoid in each spatial frequency bin. As shown in Fig. 6b, the spatial spectrum indicates a peak at 0.4 cycles/mm $(\lambda = 2.5\ \text{mm})$ with an estimated sinusoidal amplitude of $51.0\ \mu$m.

Under the assumption that the original signal variance has a Gaussian distribution, the spectral density estimate at each spatial frequency has a χ^2 distribution. The confidence interval ([40, p. 192]) for the spectral density estimate, $G(f_j)$, at each spatial frequency, f_j, is given by

$$\frac{n\hat{G}(f_j)}{\chi^2_{n,\alpha/2}} < G(f_j) < \frac{n\hat{G}(f_j)}{\chi^2_{n,1-\alpha/2}}. \tag{5}$$

Thus, following (5), the upper and lower 95 percent confidence bound $(\alpha = 0.05, n = 27)$ in Fig. 6b indicates that the sinusoidal grating's estimated amplitude of $51.0\ \mu$m (95 percent confidence interval: $40.3 - 69.5\ \mu$m) is not statistically discernible from the commanded amplitude of $50\ \mu$m.

The characteristics of the virtual triangular gratings were similarly evaluated in the spatial frequency domains. Fig. 7a shows an example of recorded $z(x)$ for a single stroke across a virtual triangle grating. The difference between triangular and sinusoidal gratings, indicated by the harmonic components in (3), is empirically evident in the spatial spectrum estimate averaged from ten repeated strokes $(n = 30$ periodograms) in Fig. 7b.

Fig. 8. The test apparatus for holding two stainless steel blocks with surface gratings. The numbers "1" and "2" were used by the experimenter to determine which grating should be presented to the left of the participant on each trial. The apparatus was always obscured by a curtain from the participant's view.

Fig. 7b indicates the stroked triangle signal grating had a measured amplitude of $40.8\ \mu\text{m}$ (95 percent confidence interval: $32.6 - 54.5\ \mu\text{m}$) at the 0.4 cycle/mm ($\lambda = 2.5$ mm) fundamental frequency, $4.7\ \mu\text{m}$ (confidence interval: $3.8 - 6.3\ \mu\text{m}$) for the third harmonic at 1.2 cycle/mm ($\lambda = 0.833$ mm), and $1.4\ \mu\text{m}$ (confidence interval: $1.1 - 1.8\ \mu\text{m}$) for the fifth harmonic at 2.0 cycle/mm ($\lambda = 0.5$ mm). Respectively, the amplitudes of the fundamental and these two harmonic components are not statistically distinguishable from their theoretically predicted levels of $8/\pi^2 \times 50\ \mu\text{m} = 40.5\ \mu\text{m}, 1/9 \times 40.5\ \mu\text{m} = 4.5\ \mu\text{m}$, and $1/25 \times 40.5\ \mu\text{m} = 1.6\ \mu\text{m}$.

2.3 Procedures

The experiments followed a two-interval two-alternative forced choice paradigm based on signal detection theory [41]. Four pairs of grating amplitudes were compared under each experimental condition (Finger real, Stylus real, and Stylus virtual) for the two grating types: $A_0(50\ \mu\text{m})$ and $A_1(55\ \mu\text{m})$, A_0 and $A_2(60\ \mu\text{m}), A_0$ and $A_3(65\ \mu\text{m})$, and A_0 and $A_4(70\ \mu\text{m})$, with A_0 serving as the reference in all pairs. Training and trial-by-trial correct-answer feedback were provided. A total of 200 trials were collect for each reference-test grating pair. During the experiments, circumaural hearing protectors (Twin Cup H10A, NRR 29; Peltor, Sweden) were worn by all participants to block auditory cues.

For the Fingertip-on-real-grating (Finger real) condition, the participants were instructed to wash their hands with soap to remove residual oils on the skin surfaces. The experimenter and the participant then sat facing each other across a table with a vertical curtain between them. The experimenter inserted two samples into a long slot (see Fig. 8). A piece of felt fabric with two openings slightly smaller than the grating surfaces (so as to mask the edges) covered the test apparatus. Before starting, it was explained to participants that they would feel two different texture samples and their task was to determine which sample felt rougher. Participants placed their dominant hand under the curtain in order to feel the gratings hidden from view. Only the fingertip of the index finger, excluding the nail, was allowed to touch the samples. Participants were free to choose the stroking speed and the amount of time spent touching the samples. Most participants adopted a back-and-forth lateral stroking pattern. For each trial, a computer program determined the presentation location of the two stimuli (reference stimulus on the left or right side). The experimenter spun the test apparatus on the table top several times regardless of whether the order of the stimuli had changed from the previous trial. The experimenter then stopped the apparatus at the desired orientation so that the grating with the higher amplitude was either on the left side (stimulus "1") or right side (stimulus "2") from the participant's viewpoint. The participant verbally responded "1" or "2" to the experimenter who then entered the response into the computer. Correct-answer feedback was provided to both the participant and the experimenter by means of two easily discernable audio tones.

Each run comprised a block of 50 trials with the same pair of gratings. The participant took a short break between runs to prevent fingertip numbness. The order of the 16 runs (4 grating pairs $\times 4$ runs/pair) per grating type was randomized for each participant. The experiment was spread over several sessions with each session lasting 1 to 2 hours, depending on participant comfort.

The procedure for the Stylus-on-real-grating (Stylus real) condition was identical to that for the Finger-real condition, except that a stylus was used to stroke the gratings as opposed to a fingertip. The stylus used for this procedure was constructed from a single piece of machined Delrin (Polyoxymethylene) to have the identical look and feel as the one on the ministick. The stylus measured 106 mm in length by 5 mm in diameter that tapered over 13 mm to a 1.6 mm (diameter) hemispherical tip at the end that contacts the grating surface.

For the Stylus-on-virtual-grating (Stylus virtual) condition, the participant stroked two virtual gratings placed side by side with a gap of 12.7 mm (0.5 in) (see the color patches in Fig. 5). Since it took much less time to present pairs of virtual gratings with the ministick, each run comprised 100 trials. Collection of complete data sets for the virtual-grating condition required, on average, 3 hours per participant per grating type compared with 9 hours for the real-grating conditions. The order of the eight runs (4 grating pairs $\times 2$ runs/pair) per grating type was randomized between participants. The participants were instructed to look away from the ministick, but no curtain was used for this condition. They were allowed to stroke the virtual gratings at any pace they felt comfortable. The participants themselves directly entered either a "1" or "2" via the computer keyboard based on location of the grating with the greater perceived roughness. Correct-answer feedback was provided by a textual display ("Correct" or "Wrong") on the computer screen.

Because of the greater time commitment involved, fewer participants were recruited for the Finger-real and Stylus-real conditions than for the Stylus-on-virtual-grating condition.

2.4 Data Analysis

For each participant, a stimulus-response matrix for each grating pair was constructed and the sensitivity index d' and response bias β were calculated [41]. To estimate the amplitude discrimination threshold (i.e., the JND—just noticeable difference) from d' values, we first calculated the slope of the best-fitting line by averaging the slopes from the d' values corresponding to the four grating pairs:

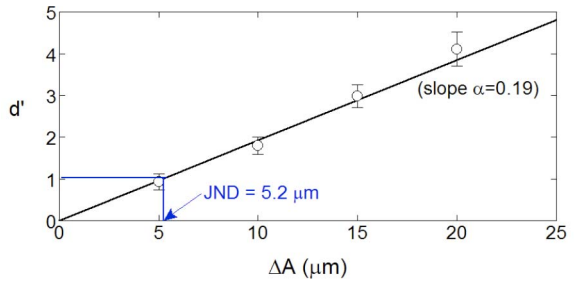

Fig. 9. Illustration of data processing scheme using fictitious data. The d′ values (± std. error) associated with the four grating pairs, plotted against ΔA, the amplitude difference between a pair of gratings, are shown. The best fitting line, its slope and estimated amplitude JND are also shown.

$$\alpha = \frac{1}{N}\sum_{i=1}^{N}\frac{d'_i}{\Delta A_i}, \tag{6}$$

where d'_i, the sensitivity index for the discrimination of A_0 and $A_i (i = 1, \ldots, 4)$, was divided by the respective difference between the reference and test grating amplitudes, $\Delta A_i = A_i - A_0$, and then averaged by N, the number of grating amplitude pairs). The "Just-Noticeable Difference" was then calculated as the amplitude difference $\Delta A = A - A_0$ for which $d' = 1$, or equivalently, $JND = 1/\alpha$ (see also [42]). This process is illustrated in Fig. 9.

2.5 Participants

Fifteen individuals (P1-P15) examined the sinusoidal gratings. Among those, four (2M/2F) took part in the Finger-real condition, four (2M/2F) in the Stylus-real condition, and seven (3M/4F) in the Stylus-virtual condition. Thirteen different participants (P16-P28) were tested with the triangular gratings. Among them, four (2M/2F) took part in the Finger-real condition, four (2M/2F) in the Stylus-real condition, and five (3M/2F) in the Stylus-virtual condition. All participants except for one (P5) were right handed and reported no known conditions that would compromise their sense of touch. Seven participants (P1, P2, P10, P18, P19, P20, P24) were laboratory research staff who had previous experience with haptic studies. The rest of the participants were remunerated for their time.

3 Results

The amplitude discrimination thresholds for sinusoidal gratings are shown in Table 1. The participants' average thresholds (mean ± standard error of mean) for a reference amplitude of $50\ \mu\text{m}$ under the Finger-real, Stylus-real, and Stylus-virtual conditions were $3.9 \pm 0.4, 2.4 \pm 0.4$, and $4.9 \pm 0.2\ \mu\text{m}$, respectively.

With a complete independent-groups design, the parametric one-way ANOVA showed that the experimental interface condition had a significant effect $(F_{2,12} = 15.192, p < 0.001)$ on discrimination thresholds for sinusoidal gratings. Posthoc Newman-Keuls contrasts indicated that this effect was due to the Stylus-real thresholds being significantly smaller than those for either the Stylus-virtual (critical difference $= 1.57\ \mu\text{m}, p < 0.01$) or Finger-real (critical difference $= 1.08\ \mu\text{m}, p < 0.05$). The thresholds for the Stylus-virtual and Finger-real conditions, however, were not significantly different from each other. Because the Gaussianess of the threshold data cannot be ascertained from our small sample size, a nonparametric (i.e., distribution free) test was used to corroborate this finding. The Kruskal-Wallis test for independent groups again indicated that the experimental condition had a significant effect ($\hat{H}_{4,4,7} = 9.953, p < 0.01$). Nonparametric (Kruskal-Wallis) post hoc contrasts, however, showed that only the Stylus-virtual and Stylus-real thresholds differed significantly from each other $(p < 0.01)$. Therefore, we conclude that the detection thresholds for sinusoidal gratings differ significantly only between the real and virtual stylus conditions but do not draw conclusions for contrasts involving the Finger-real condition.

TABLE 1
Discrimination Thresholds (in μm) by Experimental Condition for Sinusoidal Gratings

Participant	(a) Finger-real	(b) Stylus-real	(c) Stylus-virtual
P1	4.1		
P2	4.4		
P3	4.3		
P4	2.8		
P5		3.5	
P6		1.9	
P7		2.7	
P8		1.6	
P9			4.9
P10			5.8
P11			5.1
P12			4.5
P13			4.1
P14			4.3
P15			5.3
Average	**3.9**	**2.4**	**4.9**
Std. Err.	0.4	0.4	0.2

The amplitude discrimination thresholds for triangular gratings are shown in three panels for the three grating-stylus conditions in Table 2. The participants' average thresholds for the Finger-real, Stylus-real, and Stylus-virtual conditions were $3.7 \pm 0.3, 2.6 \pm 0.2$, and $4.8 \pm 0.5\ \mu\text{m}$, respectively, for a 50-μm reference amplitude.

The parametric one-way independent-groups ANOVA showed that the experimental interface condition had a significant effect $(F_{2,10} = 7.468, p < 0.02)$ on thresholds for triangular gratings. Post-hoc Newman-Keuls contrasts indicate that this effect was due to the Stylus-real thresholds being significantly smaller than those for the Stylus-virtual condition (critical difference $= 2.09\ \mu\text{m}, p < 0.01$). The other two possible threshold pairings according to interface were not significantly different from each other. The nonparametric Kruskal-Wallis test for independent groups again indicated that the experimental condition had a significant effect ($\hat{H}_{4,4,5} = 7.596, p < 0.05$), while nonparametric post hoc contrasts supported the finding that only the Stylus-virtual and Stylus-real thresholds differed significantly $(p < 0.01)$. Thus, for triangular gratings, we conclude that the real and virtual stylus conditions differ significantly but do not draw conclusions for contrasts involving the Finger-real condition.

TABLE 2
Discrimination Thresholds (in μm) by Experimental Condition for Triangular Gratings

Participant	(a) Finger-real	(b) Stylus-real	(c) Stylus-virtual
P16	3.7		
P17	4.2		
P18	4.1		
P19	2.8		
P20		2.1	
P21		2.4	
P22		2.7	
P23		3.1	
P24			3.0
P25			5.7
P26			6.1
P27			4.6
P28			4.8
Average	**3.7**	**2.6**	**4.8**
Std. Err.	0.3	0.2	0.5

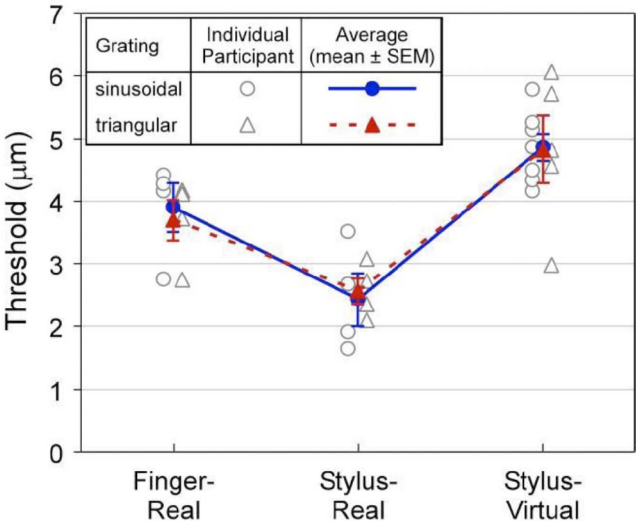

Fig. 10. Comparison of amplitude discrimination thresholds for sinusoidal (open circles) and triangular gratings (open triangles) under the three experimental conditions. Each open symbol represents one individual participant's threshold and is slightly offset for clarity. The average thresholds are shown with filled symbols.

The individual and average threshold results for both sinusoidal and triangular gratings are summarized in Fig. 10. Visual inspection indicates that while thresholds differed significantly across the three experimental conditions, there was little difference between the sinusoidal and triangular gratings. A two-way independent-groups ANOVA from pooled data again reveals a significant main effect for experimental interface condition ($F_{1,22} = 21.18; p < 0.0001$). However, neither the grating type ($F_{2,22} = 0.011; p < 0.916$) nor the interaction between grating type and experimental condition ($F_{2,22} = 0.091; p < 0.913$) were significant. When combined across the sinusoidal and triangular grating profiles, the average discrimination thresholds for the Finger-real (3.8 ± 0.2 μm), Stylus-real (2.5 ± 0.2 μm), and Stylus-virtual (4.9 ± 0.2 μm) conditions all differed significantly ($p < 0.01$) from each other according to Newman-Keuls post-hoc contrasts (Finger-real versus Stylus-real, critical difference 1.10 μm; Stylus-real versus Stylus-virtual, critical difference 1.16 μm; Finger-real versus Stylus-virtual, critical difference 1.01 μm). While the Kruskal-Wallis nonparametric test supports the observation of a significant main effect for experimental condition for the combined sinusoidal and triangular data ($H_{8,8,12} = 18.87,\ p \ll 0.01$), the accompanying nonparametric posthoc analysis indicates, however, that again only the real and virtual stylus condition thresholds differed significantly ($p < 0.01$).

4 Discussion

Our amplitude discrimination thresholds for the Finger-real condition can be compared directly with that obtained by Nefs et al. [14] where similar stimuli and methods were used. Specifically, we found a discrimination threshold of 3.9 and 3.7 μm, or 7.8 and 7.4 percent of the reference amplitude of 50 μm, for sinusoidal and triangular gratings, respectively. Nefs et al. found a discrimination threshold of 8 μm for sinusoidal gratings with a similar reference amplitude of 51.2 μm and an identical spatial-period of 2.5 mm. The smaller threshold found in the present study may be the result of a difference in the instructions given to the participants. In Nefs et al. [14] study, the participants could only stroke the textured surfaces twice from side to side, whereas in the present study participants were allowed to stroke the surfaces as many times as they wished. In our pilot tests, we had tried to limit the number of strokes to two, but found the task to be too difficult to perform. We then decided to let the participants feel the textures for as long as needed in order to determine the best achievable thresholds (personal communications with R. Klatzky and S. Lederman in 2004). A second difference is the use of feedback. In Nefs et al.'s study, feedback was given only during practice trials. In our present study, trial-by-trial correct-answer feedback was provided throughout the main experiment. Therefore, the 3.9 and 3.7 μm results from our Finger-real condition may be viewed as a *lower bound* threshold for amplitude discrimination of sinusoidal and triangular gratings with a 50 μm amplitude and a 2.5 mm spatial period. The 8 μm value from Nefs et al. [14] may be considered a *typical* threshold for amplitude discrimination of similar sinusoidal (51.2 μm amplitude) gratings.

In the Stylus-real condition, average discrimination thresholds were 2.4 and 2.6 μm, or 4.8 and 5.2 percent of the reference amplitude of 50 μm for the sinusoidal and triangular textures, respectively. Our finding, that amplitude discrimination thresholds for texture gratings were marginally (i.e., by parametric but not by nonparametric statistical analyses) higher for the Finger-real condition than for the Stylus-real condition, is perhaps counterintuitive considering the fact that more information is available through direct fingerpad exploration than probe-mediated exploration of textures [11], [12]. The real textures, when explored with the bare finger, convey spatial (size of microstructures) and intensive (depth of microstructures) information as well as temporal (vibration) information

arising from lateral stroking of the grating. During normal active touch (i.e., during volitional limb movement) with the bare skin, observers rely mainly on spatial-intensive information and can ignore vibratory frequencies to judge texture intensity (i.e., roughness). The virtual texture, on the other hand, can only be experienced via the mechanical vibration of the haptic interface linkage produced by the interaction between the stylus's virtual tip and texture as the grating is stroked. As is the case for exploring the real textures with a rigid stylus, observers can make use of vibratory sensations caused by stylus-grating interaction in conjunction with the kinesthetic feedback from their movement to judge texture intensity. One might thus expect that the thresholds for the Finger-real condition be lower than those for the Stylus-real condition. However, according to the following paragraph, sensory desensitizing/adaptation might have played a bigger role in the Finger-real condition than in the Stylus-real condition.

There may be several reasons why the thresholds obtained with the stylus are lower than those obtained with the fingerpad for real texture samples. First, even though care was taken to ensure breaks between runs in the Finger-real condition, it was still possible that the fingerpad was becoming slightly desensitized from the repeated rubbing against the stainless steel surfaces. Second, the contact area between the stylus and the hand with the Stylus-real condition was spread across the fingerpads of the thumb, index, and middle fingers, resulting in a larger total contact area for detection of temporal vibration patterns. Previous studies have shown that larger contact area can lead to lower thresholds (e.g., [43], [44]). Third, according to anecdotal notes, the Stylus-real condition led to "crisper" or "sharper" sensations than the Finger-real condition. The strong vibrations transmitted by the probe from stroking the textured surfaces might have made it easier to discriminate the roughness between pairs of textures.

In the Stylus-virtual condition, average amplitude discrimination thresholds of 4.9 and $4.8\ \mu\mathrm{m}$ (9.8 and 9.6 percent of the reference amplitude of $50\ \mu\mathrm{m}$) were found for the sinusoidal and triangular textures, respectively. This value can be compared to results from a series of experiments on haptic texture perception using force-feedback devices [15], [16], [45], [46], [47], [48]. Our Stylus-virtual sinusoidal condition is similar to Weisenberger and Krier's study [45] where 2D sinusoidal "bumps" were simulated on a PHANToM force-feedback device. They estimated amplitude JNDs over a range of amplitude and spatial frequency values. For gratings with a spatial frequency of 3.88 cycles/cm, which is close to the 2.5 mm (4 cycles/cm) wavelength of the present study of 1D gratings, they found JNDs of roughly 0.15 mm (25-12.5 percent of the reference) for a 0.6-1.2 mm reference amplitude range. Thus, even though Weisenberger and Krier's [45] stimulus amplitudes were 10-20 times larger than ours, when expressed as Weber fractions, our results for the Stylus-virtual condition and their smaller Weber fractions are roughly comparable considering the many differences in stimuli, apparatus, and experimental procedures between the two studies.

A possible explanation for better performance in the Stylus-real condition than the Stylus-virtual condition is the difference in surface stiffness. Touching of real and virtual surfaces is inherently different. Specifically, a real stainless steel surface has an almost infinite stiffness and cannot be penetrated by the stylus, whereas an impedance implementation of a virtual surface has a limited stiffness and must be penetrated by a virtual stylus before it can be perceived. The latter results in movement profiles that "drift" slightly in the height direction (z-axis) of the grating profiles (see Figs. 6a and 7a). This might have affected the participants' ability to discriminate the amplitudes of pairs of sinusoidal or triangular gratings as effectively in the Stylus-virtual condition as in the Stylus-real condition. Another factor is that, unlike the real textures, the method we employed for rendering both virtual sinusoidal and triangular gratings, expressed by (4), offers resistance to surface penetration but no tangential resistance, i.e., friction. However, despite the many differences between the experiments on real and virtual textures, the thresholds are actually remarkably similar (i.e., within a factor of 2). Future studies will investigate this issue further by increasing the stiffness constant in (4) in the rendering algorithm.

Regardless of the experimental interface condition, the discrimination thresholds obtained for the sinusoidal and triangular gratings were not statistically distinct. There are two possible explanations for this finding. One possibility is that the spatial harmonic components of the triangular gratings were not sufficiently strong to contribute to the perception of a triangular grating. Thus, the triangular gratings used in the present study felt like sinusoidal gratings and one would expect similar amplitude discrimination thresholds for both types of gratings. This turned out not to be the case because the third harmonic component of a 50-μm triangular grating has an amplitude of $4.5\ \mu\mathrm{m}$ at a spatial frequency of 1.2 cycle/mm, which is above the detection threshold of $1.9\ \mu\mathrm{m}$ for a sinusoidal component at a similar spatial frequency of 1.25 cycle/mm reported in [20]. Therefore, the findings of Cholewiak et al. [20] would have predicted that the triangular gratings used in the present study should feel different from the sinusoidal gratings used in the present study. A second explanation is that the differences in the amplitudes of the harmonic components of the triangular gratings used in the present study, whether they were real or virtual, were below human discrimination thresholds and therefore did not contribute to the overall amplitude discrimination task for triangular gratings. There are no experimental data available at this time to assess the second explanation. A future study could involve direct comparisons of sinusoidal and triangle grating stimuli to discern whether spatial harmonics have a role in establishing the different percepts.

Klatzky and Lederman [49] demonstrated that participants perceived raised dot textures with smaller interelement (i.e., dot) spacing as being rougher when experienced with a smaller than a larger diameter probe tip, and least rough with the bare finger tip. But, as interelement spacing was increased, the ordering of perceived roughness by probe sizes and fingertip was reversed. Equating interelement spacing between raised dots with the spacing between our textures' ridges would indicate that the crossover in Klatzky and Lederman's roughness ordering occurred approximately at the wavelength of our sinusoidal and triangular gratings. While increased subjective roughness ratings in Klatzky and Lederman's study can be expected to correspond to higher sensitivity and lower threshold, predicting whether the finger or stylus should produce

smaller thresholds in our present experiments is difficult for two reasons. First, as noted above, there is a probe tip diameter dependent crossover in roughness ratings [12], [49], suggesting that threshold magnitudes should be comparable for the finger and probe (stylus) near the wavelength of our textures. Second, the probe tip in our Stylus-virtual condition is modeled as a simple point that has a zero diameter. Extrapolating from the two probe tip diameters in Klatzky and Lederman's study [49] down to our virtual tip's zero diameter might lead one to expect the roughness rating crossover point to shift to a lower interelement spacing than our present grating wavelength. Such a shift would make the perceived roughness greater and, therefore, the threshold lower for the finger than for the virtual probe. However, we are unable to conclude a statistically significant difference between the thresholds obtained with the bare fingertip and those with the stylus.

Finally, a main motivation of the present study was to investigate the efficacy of virtual gratings in studying human texture perception. A recent study by Unger et al. [23], using a six-axis magnetic levitation haptic device for virtual textured haptic surfaces, demonstrated similar psychophysical functions for roughness magnitude estimation of real and virtual textures when probe geometry and velocity were taken into account in the virtual texture model. The results of the present study indicate a twofold difference between the amplitude discrimination thresholds obtained with a stylus on real gratings $(2.5\ \mu\mathrm{m})$ and those on virtual gratings $(4.9\ \mu\mathrm{m})$. The larger thresholds associated with the virtual gratings could be due to the limited stiffness of the virtual surfaces that resulted in variable peak-trough distances traveled by the probe (compare Figs. 6a and 7a with the top panels of Figs. 2 and 3, respectively) when stroking the virtual gratings. Also, as noted above, our virtual textures did not provide tangential resistance forces (i.e., parallel to the stroke direction). Furthermore, even though every effort was made to use the same psychophysical testing protocol with both real and virtual surfaces, it appeared that the participants put in more effort with real texture gratings when the experimenter presented and recorded every trial and the correct-answer feedback signal could be heard by both the experimenter and the participant. Overall, the thresholds obtained in the present study are very similar considering the several differences between the Finger-real, Stylus-real, and Stylus-virtual experimental conditions.

Our results should be viewed in the context of the specific conditions employed in the present study. For example, our study focused on the perception of surface roughness due to grating amplitudes. It is known that friction (or stickiness) also plays an important role in haptic texture perception [5], [29]. Future work needs to carefully assess the extent to which lateral force profiles can be successfully simulated with a haptic device. In addition, the gratings used in the present study do not reflect the complexity of surface textures encountered in our daily lives. Other factors, such as surface stiffness and thermal properties, all need to be taken into account when studying haptic texture perception.

What is emerging from the present as well as our previous studies is the extraordinary sensitivity of human skin to the vibrations resulting from stroking a surface with microgeometric height variations, i.e., differences on the order of microns. By conducting parallel experiments with high-definition real textures and virtual surfaces rendered by a high spatial-resolution force-feedback device, we have shown that, like the magnetic levitation haptic device [23], the ministick is a useful experimental platform for studying human texture perception. In addition to the repeated upfront costs associated with the fabrication of new *real* stimuli at the onset of a perceptual study, the use of *real* surface textures also entails the relatively cumbersome manual exchange of specimens during the experiment. Thus, *virtual* textures rendered by very high performance haptic interfaces open the door to a wide range of studies that otherwise could not have been conducted easily, quickly, or economically (e.g., [20], [23]). We hasten to point out, however, that due to the different perceptual cues that are available from using a finger and a stylus, care should be taken when comparing results obtained with the bare fingertip and those with the stylus. Finally, a direct comparison of the results under the Stylus-Real and Stylus-Virtual conditions indicates that performance was better (i.e., thresholds were lower) for real gratings than for virtual gratings, at least as rendered with the current ministick. Further empirical and theoretical studies are needed to develop better virtual models that capture the essential properties of real gratings.

Acknowledgments

This work was supported in part by a US National Science Foundation Award under Grant No. 0098443-IIS, and in part by NASA under award no. NCC 2-1363. In addition, Matthew Kocsis was partially supported by a graduate fellowship from the School of Electrical and Computer Engineering at Purdue University. The authors thank Drs. Susan Lederman and Roberta Klatzky for discussions on experimental methods, Mike Sherwood at Purdue University for his assistance with the fabrication of the EDM samples with surface gratings, Patrick Kalita for the spectral analysis of virtual texture gratings shown in Figs. 6 and 7, and Dr. Michael Seaman at the University of South Carolina for providing the extended Kruskal-Wallis tables for some of the statistical analyses. Portions of this paper reprinted with permission from [36] and [35], © 2006/2007 IEEE.

References

[1] D. Katz, *The World of Touch.* Lawrence Erlbaum Assoc., 1989.
[2] R.H. LaMotte and M.A. Srinivasan, "Tactile Discrimination of Shape: Responses of Slowly Adapting Mechanoreceptive Afferents to a Step Stroked Across the Monkey Fingerpad," *The J. Neuroscience,* vol. 7, pp. 1655-1671, 1987a.
[3] R.H. LaMotte and M.A. Srinivasan, "Tactile Discrimination of Shape: Responses of Rapidly Adapting Mechanoreceptive Afferents to a Step Stroked Across the Monkey Fingerpad," *The J. Neuroscience,* vol. 7, pp. 1672-1681, 1987.
[4] C.E. Connor, S.S. Hsiao, J.R. Phillips, and K.O. Johnson, "Tactile Roughness: Neural Codes that Account for Psychophysical Magnitude Estimates," *J. Neuroscience,* vol. 10, pp. 3823-3836, 1990.
[5] M. Hollins, R. Faldowski, S. Rao, and F. Young, "Perceptual Dimensions of Tactile Surface Texture: A Multidimensional Scaling Analysis," *Perception & Psychophysics,* vol. 54, pp. 697-705, 1993.
[6] R.L. Klatzky, S.J. Lederman, C. Hamilton, M. Grindley, and R.H. Swendsen, "Feeling Textures through a Probe: Effects of Probe and Surface Geometry and Exploratory Factors," *Perception & Psychophysics,* vol. 65, pp. 613 - 631, 2003.

[7] S.S. Stevens and J.R. Harris, "The Scaling of Subjective Roughness and Smoothness," *J. Experimental Psychology,* vol. 64, pp. 489-494, 1962.

[8] S.J. Lederman and M.M. Taylor, "Fingertip Force, Surface Geometry, and the Perception of Roughness by Active Touch," *Perception & Psychophysics,* vol. 12, pp. 401 - 408, 1972.

[9] S.J. Lederman, "Tactile Roughness of Grooved Surfaces: The Touching Process and Effects of Macro- and Microsurface Structure," *Perception & Psychophysics,* vol. 16, pp. 385-395, 1974.

[10] S.J. Lederman, G. Thorne, and B. Jones, "Perception of Texture by Vision and Touch: Multidimensionality and Intersensory Integration," *J. Experimental Psychology: Human Perception and Performance,* vol. 12, pp. 169-180, 1986.

[11] C.E. Connor and K.O. Johnson, "Neural Coding of Tactile Texture: Comparison of Spatial and Temporal Mechanisms for Roughness Perception," *J. Neuroscience,* vol. 12, pp. 3414-3426, 1992.

[12] S.J. Lederman, R.L. Klatzky, C.L. Hamilton, and G.I. Ramsay, "Perceiving Roughness via a Rigid Probe: Psychophysical Effects of Exploration Speed and Mode of Touch," *Haptics-e: The Electronic J. Haptics Research,* vol. 1, pp. 1-20, http://www.haptics-e.org, 1999.

[13] S. Louw, A.M.L. Kappers, and J.J. Koenderink, "Haptic Detection Thresholds of Gaussian Profiles over the Whole Range of Spatial Scales," *Experimental Brain Research,* vol. 132, pp. 369-374, 2000.

[14] H.T. Nefs, A.M.L. Kappers, and J.J. Koenderink, "Amplitude and Spatial-Period Discrimination in Sinusoidal Gratings by Dynamic Touch," *Perception,* vol. 30, pp. 1263-1274, 2001.

[15] J.M. Weisenberger, M.J. Krier, and M.A. Rinker, "Judging the Orientation of Sinusoidal and Square-Wave Virtual Gratings Presented via 2-DOF and 3-DOF Haptic Interfaces," *Haptics-e: The Electronic J. for Haptics Research,* vol. 1, http://www.haptics-e.org,, 2000.

[16] P.P. Ho, B.D. Adelstein, and H. Kazerooni, "Judging 2D Versus 3D Square-Wave Virtual Gratings," *Proc. 12th Int'l Symp. Haptic Interfaces for Virtual Environment and Teleoperator Systems (HAPTICS '04),* pp. 176- 183, 2004.

[17] S. Choi and H.Z. Tan, "Perceived Instability of Virtual Haptic Texture. II. Effect of Collision Detection Algorithm," *Presence: Teleoperators and Virtual Environments,* vol. 14, pp. 463-481, 2005.

[18] L.B. Rosenberg and B.D. Adelstein, "Perceptual Decomposition of Virtual Haptic Surfaces," *Proc. IEEE Symp. Research Frontiers in Virtual Reality,* pp. 46-53, 1993.

[19] D.A. Lawrence, L.Y. Pao, A.M. Dougherty, M.A. Salada, and Y. Pavlou, "Rate-Hardness: A New Performance Metric for Haptic Interface," *IEEE Trans. Robotics and Automation,* vol. 16, no. 4, pp. 357-371, Aug. 2000.

[20] S.A. Cholewiak, K. Kim, H.Z. Tan, and B.D. Adelstein, "A Frequency-Domain Analysis of Haptic Gratings," *IEEE Trans. Haptics,* vol. 3, no. 1, pp. 3-14, Jan.-Mar. 2010.

[21] P. Buttolo, D. Kung, and B. Hannaford, "Manipulation in Real, Virtual, and Remote Environments," *Proc. IEEE Int'l Conf. Systems, Man, and Cybernetics,* vol. 5, pp. 4656-4661, Oct. 1995.

[22] B.J. Unger, A. Nicolaidis, P.J. Berkelman, A. Thompson, S. Lederman, R.L. Klatzky, and R.L. Hollis, "Virtual Peg-in-Hole Performance Using a 6-DOF Magnetic Levitation Haptic Device: Comparison with Real Forces and with Visual Guidance Alone," *Proc. 10th Int'l Symp. Haptic Interfaces for Virtual Environment and Teleoperator Systems,* pp. 263-270, 2002.

[23] B. Unger, R. Hollis, and R. Klatzky, "Roughness Perception in Virtual Textures," *IEEE Trans. Haptics,* vol. 4, no. 2, pp. 122-133, Mar./Apr. 2011.

[24] A.M. West and M.R. Cutkosky, "Detection of Real and Virtual Fine Surface Features with a Haptic Interface and Stylus," *Proc. ASME Systems and Control Division,* vol. 61, pp. 159-166, 1997.

[25] S. Greenish, V. Hayward, V. Chial, A. Okamura, and T. Steffen, "Measurement, Analysis, and Display of Haptic Signals During Surgical Cutting," *Presence: Teleoperators and Virtual Environments,* vol. 11, pp. 626-651, 2002.

[26] M.K. O'Malley and M. Goldfarb, "On the Ability of Humans to Haptically Identify and Discriminate Real and Simulated Objects," *Presence: Teleoperators and Virtual Environments,* vol. 14, pp. 366-376, 2005.

[27] Y. Ikei and M. Shiratori, "TextureExplorer: A Tactile and Force Display for Virtual Textures," *Proc. Symp. Haptic Interfaces for Virtual Environment and Teleoperator Systems (HAPTICS '02),* pp. 327 - 334, 2002.

[28] K.-U. Kyung, S.-W. Son, G.-H. Yang, and D.-S. Kwon, "How to Effectively Display Surface Properties Using an Integrated Tactile Display System," *Proc. IEEE Int'l Conf. Robotics and Automation,* pp. 1761-1766, 2005.

[29] G. Campion, A.H.C. Gosline, and V. Hayward, "Does Judgement of Haptic Virtual Texture Roughness Scale Monotonically with Lateral Force Modulation?" *EuroHaptics '08: Proc. Sixth Int'l Conf. Haptics: Perception, Devices and Scenarios,* pp. 718-723, 2008.

[30] R. Samra, D. Wang, and M.H. Zadeh, "Design and Evaluation of a Haptic Tactile Actuator to Simulate Rough Textures," *Proc. IEEE Virtual Reality Conf. (VR '10),* pp. 301-302, 2010.

[31] R. Samra, D. Wang, and M.H. Zadeh, "On Texture Perception in a Haptic-Enabled Virtual Environment," *Proc. IEEE Int'l Symp. Haptic Audio-Visual Environments and Games (HAVE '10),* pp. 1-4, 2010.

[32] S. Choi and H.Z. Tan, "Perceived Instability of Virtual Haptic Texture. I. Experimental Studies," *Presence: Teleoperators and Virtual Environments,* vol. 13, pp. 395-415, 2004.

[33] S. Choi and H.Z. Tan, "Perceived Instability of Virtual Haptic Texture. III. Effect of Update Rate," *Presence: Teleoperators & Virtual Environments,* vol. 16, pp. 263-278, 2007.

[34] B. Unger, R. Hollis, and R. Klatzsky, "The Geometric Model for Percieved Roughness Applies to Virtual Textures," *Proc. Symp. Haptic Interfaces for Virtual Environment and Teleoperator Systems (HAPTICS '08),* pp. 3-10, 2008.

[35] M. Kocsis, H.Z. Tan, and B.D. Adelstein, "Discriminability of Real and Virtual Surfaces with Triangular Gratings," *Proc. Second Joint EuroHaptics Conf. and Symp. Haptic Interfaces for Virtual Environment and Teleoperator Systems (WHC '07),* pp. 348-353, 2007.

[36] H.Z. Tan, B.D. Adelstein, R. Traylor, M. Kocsis, and E.D. Hirleman, "Discrimination of Real and Virtual High-Definition Textured Surfaces," *Proc. 14th Int'l Symp. Haptic Interfaces for Virtual Environment and Teleoperator Systems (HAPTICS '06),* pp. 3-9, 2006.

[37] R. Traylor, D. Wilhelm, B.D. Adelstein, and H.Z. Tan, "Design Considerations for Stand-Alone Haptic Interfaces Communicating via UDP Protocol," *Proc. World Haptics Conf. (WHC '05): The First Joint EuroHaptics Conference and the Symp. Haptic Interfaces for Virtual Environment and Teleoperator Systems,* pp. 563-564, 2005.

[38] B.D. Adelstein, "Three Degree of Freedom Parallel Mechanical Linkage," US Patent no. 5,816,105, Oct. 1998.

[39] R. Steger, K. Lin, B.D. Adelstein, and H. Kazerooni, "Design of a Passively Balanced Spatial Linkage Haptic Interface," *ASME J. Mechanical Design,* vol. 126, pp. 984-991, 2004.

[40] J.S. Bendat and A.G. Piersol, *Random Data: Analysis and Measurement Procedures.* Wiley, 2010.

[41] N.A. Macmillan and C.D. Creelman, *Detection Theory: A User's Guide,* second ed. Lawrence Erlbaum Assoc., 2004.

[42] X.-D. Pang, H.Z. Tan, and N.I. Durlach, "Manual Discrimination of Force Using Active Finger Motion," *Perception & Psychophysics,* vol. 49, pp. 531-540, 1991.

[43] R.T. Verrillo and G.A. Gescheider, "Perception via the Sense of Touch," *Tactile Aids for the Hearing Impaired,* chapter 1, I.R. Summers, ed., pp. 1-36, Whurr Publishers, 1992.

[44] A.J. Brisben, S.S. Hsiao, and K.O. Johnson, "Detection of Vibration Transmitted through an Object Grasped in the Hand," *J. Neurophysiology,* vol. 81, pp. 1548-1558, 1999.

[45] J.M. Weisenberger and M.J. Krier, "Haptic Perception of Simulated Surface Textures via Vibratory and Force Feedback Displays," *Proc. ASME Dynamic Systems and Control Division,* vol. 61, pp. 55-60, 1997.

[46] J.M. Weisenberger, M.J. Krier, and M.A. Rinker, "Resolution of Virtual Grating Orientation with 2-DOF and 3-DOF Force Feedback Systems," *Proc. ASME Dynamic Systems and Control Division,* vol. 64, pp. 295-301, 1998.

[47] J.M. Weisenberger, M.J. Krier, M.A. Rinker, and S.M. Kreidler, "The Role of the End-Effector in the Perception of Virtual Surfaces Presented via Force-Feedback Haptic Interfaces," *Proc. ASME Dynamic Systems and Control Division,* vol. 67, pp. 35-41, 1999.

[48] G.L. Poling and J.M. Weisenberger, "Multisensory Roughness Perception of Virtual Surfaces: Effects of Correlated Cues," *Proc. 12th Int'l Symp. Haptic Interfaces for Virtual Environment and Teleoperator Systems (HAPTICS '04),* pp. 161- 168, 2004.

[49] R.L. Klatzky and S.J. Lederman, "Tactile Roughness Perception with a Rigid Link Interposed Between Skin and Surface," *Perception & Psychophysics,* vol. 61, pp. 591-607, 1999.

Matthew B. Kocsis received the bachelor's degree in computer engineering in 2006 and the master's degree in electrical and computer engineering in 2011 from Purdue University. He is currently a software engineer at Aircell, working on next generation Iridium terminal products for business aviation. He is a member of the IEEE, the IEEE Communications Society, and the IEEE Computer Society.

Steven A. Cholewiak received the bachelor's degree in psychology and physics, in 2006, from the University of Virginia (UVA) and the master's of science degree in psychology from Rutgers University, in 2010. During the undergraduate study at UVA, he was a research assistant at Gerald Clore's Social Psychology Laboratory, Timothy Salthouse's Cognitive Aging Laboratory, and Dennis Proffitt's Perception Laboratory. After graduation, he worked as a research associate at the Haptic Interface Research Laboratory with Hong Z. Tan at Purdue University. He is currently a Cognitive Psychology and Perceptual Science PhD candidate at Rutgers University working with Manish Singh. He has published one peer-reviewed journal article, two peer-reviewed conference papers, and two posters under the study of Hong Z. Tan. In addition, he has coauthored two articles and four posters while at Rutgers University. His current research focuses on modeling haptic and visual 3D shape perception.

Ryan M. Traylor received the bachelor's degree in electrical engineering and the master's degree in electrical and computer engineering from Purdue University in 2001 and 2005, respectively. He worked as a research assistant for seven years in Hong Z. Tan's Haptic Interface Research Laboratory. He is currently a principal research scientist at Battelle Memorial Institute, where he designs, builds, and fields ultrahigh speed instrumentation to support the United States Missile Defense Program. He has published six peer-reviewed conference papers, one journal article, one poster, and holds two patents.

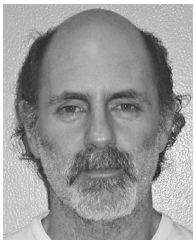

Bernard D. Adelstein received the PhD degree in 1989, in mechanical engineering from the Massachusetts Institute of Technology. He has been with the Human Systems Integration Division at the NASA Ames Research Center since 1991. He cofounded (with Ed Colgate) the ongoing annual Haptics Symposium in 1992 and was on the editorial board of the journal *Presence* from 1997 to 2006. His research centers on the assessment of human performance in multimodal virtual environments. From 2007 to 2010, he led NASA assessments of launch vibration impacts on astronaut performance. He is a senior member of the IEEE, and a member of ASME, Sigma Xi, and AAAS.

E. Daniel Hirleman received the BSME degree with Highest Distinction in 1972, the MSME degree in 1974, and the PhD degree in 1977 from Purdue University. He joined the Arizona State University faculty and also served in administrative positions culminating in associate dean for research in the College of Engineering. In 1999, he rejoined Purdue as William E. and Florence E. Perry head of ME until 2010 when he became the dean of the School of Engineering at the University of California, Merced. He received the Hon. George Brown Award for International Scientific Cooperation from the US Civilian Research & Development Foundation (CRDF) in 2008 and the Charles Russ Richards Memorial Award from Pi Tau Sigma/ASME in 2009. He chaired the International Congress on Optical Particle Sizing, served as Topical Editor for *Applied Optics*, and chairs the Engineers for a Sustainable World Advisory Board. His research involves optical sensors for surface characterization, semiconductor manufacturing, particle and flow diagnostics, biohazard detection, food safety, and global engineering education. He is a fellow of the ASME.

Hong Z. Tan received the bachelor's degree in biomedical engineering, in 1986, from Shanghai Jiao Tong University and the master's and doctorate degrees, in 1988 and 1996, respectively, both in electrical engineering and computer science, from the Massachusetts Institute of Technology (MIT). She was a research scientist at the MIT Media Lab from 1996 to 1998 before joining the faculty at Purdue University. She is currently a professor of electrical and computer engineering, with courtesy appointments in the School of Mechanical Engineering and the Department of Psychological Sciences. She founded and directs the Haptic Interface Research Laboratory at Purdue University. She is currently an editor-in-chief of the World Haptics Conference editorial board. She served as the founding chair of the IEEE Technical Committee on Haptics from 2006 to 2008. She was a recipient of the US National Science Foundation (NSF) CAREER award from 2000 to 2004. Her research focuses on haptic human-machine interfaces in the areas of haptic perception, rendering and multimodal performance. She is a senior member of the IEEE.